Numerical studies of driven, chirped Bernstein, Greene, and Kruskal modes

F. Peinetti
University of California, Berkeley, California 94720 and Politecnico di Torino, Torino, Italy

W. Bertsche, J. Fajans, and J. Wurtele
University of California, Berkeley, Berkeley, California 94720

L. Friedland
Racah Institute of Physics, Hebrew University of Jerusalem, Jerusalem 91904, Israel

Recent experiments showed the possibility of creating long-lived, nonlinear kinetic structures in a pure-electron plasma. These structures, responsible for large-amplitude periodic density fluctuations, were induced by driving the plasma with a weak oscillating drive, whose frequency was adiabatically decreased in time [W. Bertsche, J. Fajans, and L. Friedland, Phys. Rev. Lett. **91**, 265003 (2003)]. A one-dimensional analytical model of the system was developed [L. Friedland, F. Peinetti, W. Bertsche, J. Fajans, and J. Wurtele, Phys. Plasmas **11**, 4305 (2004)], which pointed out the phenomenon responsible for the modifications induced by the weak drive in the phase-space distribution of the plasma (initially Maxwellian). In order to validate the theory and to perform quantitative comparisons with the experiments, a more accurate description of the system is developed and presented here. The new detailed analysis of the geometry under consideration allows for more precise simulations of the excitation process, in which important physical and geometrical parameters (such as the length of the plasma column) are evaluated accurately. The numerical investigations probe properties and features of the modes not accessible to direct measurement. Due to the presence of two distinct time scales (because of the adiabatic chirp of the drive frequency), a fully two-dimensional numerical study of the system is expected to be rather time consuming. This becomes particularly important when, as here, a large number of comparisons (covering a wide range of drive parameters) are performed. For this reason, a coupled one-dimensional, radially averaged model is derived and implemented in a particle-in-cell code. © *2005 American Institute of Physics*. [DOI: 10.1063/1.1928251]

I. INTRODUCTION

In 1957, Bernstein, Green, and Kruskal[1] predicted the existence of a broad class of nontrivial wave solutions of the Vlasov–Poisson equations. These equilibrium solutions, known today as Bernstein–Greene–Kruskal (BGK) modes, are strongly related to the existence of trapped particles in the self-consistent electrostatic potential. However, despite the remarkable experimental effort, the generation of large-amplitude BGK modes has proven difficult;[2–5] in fact, it is generally hard to reproduce the correct initial conditions for the particle velocity distribution in the experiments. However, it is relatively easy to create *transient*, large-amplitude kinetic structures in plasmas. These waves are usually strongly Landau damped; however, if destabilizing mechanisms such as the sideband instability[6] are properly suppressed in the experiments, the asymptotic, nonlinear evolution of the Landau damping can lead to the local relaxation of the distribution to a low-amplitude BGK mode.[7]

Recently (Refs. 8 and 9), an external, chirped frequency perturbing potential was successfully used to generate and control high-amplitude BGK waves in a pure-electron plasma confined in a Malmberg–Penning trap. By using a low-amplitude, chirped-frequency drive, large density oscillations in the plasma (with $\Delta n/n$ up to $\sim40\%$) have been induced, lasting for thousands of bounce periods after the drive is switched off. These constitute the reported BGK modes.[8] The experiments showed that these large responses from the plasma are very robust and that they can be excited within a wide range of different drive parameters. Moreover, a large excitation of the system could be achieved only if the plasma temperature was sufficiently high, $T_e \gtrsim 6$ eV, i.e., in a range of temperatures where other modes (Trivelpiece–Gould modes[10]) are strongly Landau damped.[8] On the contrary, if $T_e \lesssim 1$ eV, no significant response to the frequency sweep was measured.

The excitation mechanism can be summed up as follows: the initial drive frequency $\omega_d(t=0)$ is properly chosen so that a trapped population of resonant particles (i.e., having velocity $v_p \sim \omega_d/k_d$, k_d being the drive wave number, and with the proper phase relation with respect to the drive) is created in the tail of the velocity distribution. Then, if the drive frequency is decreased in time slowly enough (k_d is fixed by the trap geometry), the resonant particles, which are trapped in the drive potential, remain phase locked to the drive and, thus, are adiabatically dragged to lower velocities and into the bulk of the distribution. To first approximation, in this process no particles can cross the separatrix between trapped and untrapped populations.[9] This means that, during the

frequency-sweeping process, the initially trapped particles are slowed down towards smaller velocities, while a larger number of particles are "pushed" over the separatrix. A similar phenomenon in accelerators is known as phase-displacement acceleration. The driving process leads eventually to a localized "hole" in phase space, which is responsible for density fluctuations of increasing amplitude as the low-density trapped population is dragged into the bulk of the distribution.

In a previous paper,[9] we proposed a one-dimensional analytical model for the system that predicted important features of the excitation process. In the first part of that work, a single-particle picture of the system was described, and the conditions under which the excitation of these structures can occur were derived. In particular, the single-particle analysis pointed out the existence of a threshold in the sweep rate for a given drive amplitude, beyond which no structures can be induced in the plasma. The model was also made self-consistent and the one-dimensional Vlasov–Poisson system was analyzed to study the experimentally observed effects of the plasma temperature on the excitation process. These analytical results predicted qualitatively the features observed in the experiments, and were also validated by comparisons with the results of one-dimensional particle-in-cell (PIC) simulations (based on the same simple model). Nonetheless, quantitative comparisons with the experiments were not performed, due to uncertainties in important geometrical and physical parameters of the system, such as the length of the plasma column and the amplitude of the drive harmonics. These two quantities have to be evaluated precisely, as they both determine the range of velocities resonant with the drive and hence affect the amplitude of the response for a given frequency sweep. For this reason, in order to perform comparisons with the experiments, a more accurate model of the system had to be developed. In order to have an accurate estimate of the plasma axial length, one needs to study the real profile of the potential well confining the plasma and of the initial equilibrium density distribution. Moreover, an accurate study of the drive potential can allow for a precise estimate of the amplitude of the different drive harmonics, otherwise not attainable. Finally, the presence of the grounded electrode that surrounds the plasma needs to be taken into account more precisely in the Poisson equation.

For these purposes, a fully two-dimensional (2D) PIC code could be employed, but, as the excitation process occurs on a time scale which is very slow compared to the bounce period of the electrons, a two-dimensional study of the system is rather time consuming. This becomes important especially if one is interested in comparing the results of simulations with experiments over a large range of variation of driving parameters. Furthermore, given the strongly magnetized nature of the electron motion inside the trap, a fully two-dimensional simulation may not be required for the particle motion.

Starting from these considerations, our aim is to present a more precise model of the system, which allows for efficient, realistic numerical simulations of the excitation process of BGK modes in a pure-electron plasma.

II. MATHEMATICAL MODELING OF THE SYSTEM

The Penning trap[8] is made of a sequence of ten cylindrical gates, of different lengths, with radius $r_w = 1.905$ cm and with a total length $L \simeq 42$ cm. The two end electrodes are biased to a negative potential ($V \sim -100$ V), while the others are grounded. This creates a potential well that provides the axial confinement of the plasma; radial confinement is provided by an axial magnetic field ($B_0 \sim 1.5 \times 10^3$ G). In the experiments, a weak oscillating potential (≈ 0.1 V) is applied to a different gate, located on one side of the trap, next to one end electrode, to drive the plasma.

The density in the center of the trap (i.e., at $r \lesssim r_p$, $z \sim L/2$) is taken to be 10^7 cm^{-3}, as measured in the experiments; this gives a total charge inside the trap of $\approx 4 \times 10^8$ electrons. The initial equilibrium density profile is obtained by assuming the plasma to be in thermal equilibrium in z, at each radius $r \lesssim r_p$:

$$n_0(r,z) = \int f_0(r,z,v_z) dv_z = \frac{N_0 g(r)\exp\left(\dfrac{e\Phi}{kT_e}\right)}{\displaystyle\int \exp\left(\dfrac{e\Phi}{kT_e}\right) dz}, \quad (1)$$

where Φ is the sum of the self-consistent potential ϕ and the potential induced by the end electrodes, ϕ_w. In Eq. (1), $g(r)$ is a function defining the radial profile of the distribution and N_0 is fixed by the required density in the center of the trap. Thus, a nonlinear Poisson equation must be solved to determine the initial plasma profile. In Fig. 1, the initial density distribution is reported for a plasma temperature of $T_e = 6$ eV, along with a (r,z) plot of the potential well confining the plasma and of the drive potential. The density distribution is, at first approximation, a step function in r, the plasma column having a radius $r_p = r_w/3$ and the z-integrated density assumed constant inside the column. As expected, the plasma density is almost independent of z in the center of the trap and drops quickly to zero near the two end electrodes over a distance $\Delta z \sim r_w$, which is the characteristic length for the exponential decrease (from 0 V to −100 V) of the confining potential in those regions of the trap. Figure 1(c) shows that the length of the plasma column L_p is much less than L, $L_p \approx 34$ cm.

Due to the presence of the strong axial magnetic field, the motion of the electrons can be regarded as a one-dimensional axial bounce motion along the magnetic field lines (the guiding-center approximation is considered). The radial electric fields are responsible for a slow $\mathbf{E} \times \mathbf{B}$ drift of the electrons. The initial distribution is azimuthally symmetric, and the $\mathbf{E} \times \mathbf{B}$ drift has no radial component. As long as azimuthal symmetry is maintained (i.e., the system must be stable to azimuthal perturbations), electrons remain at fixed radii and any slow rotation does not influence the longitudinal dynamics. For these reasons, the radial transport of particles is negligible on the time scale of interest, and the system of equations describing the evolution of the plasma can be reduced to

$$\frac{\partial f}{\partial t} + v_z \frac{\partial f}{\partial z} + \frac{e}{m_e}\frac{\partial}{\partial z}(\phi + \phi_{dr} + \phi_w)\frac{\partial f}{\partial v_z} = 0, \quad (2)$$
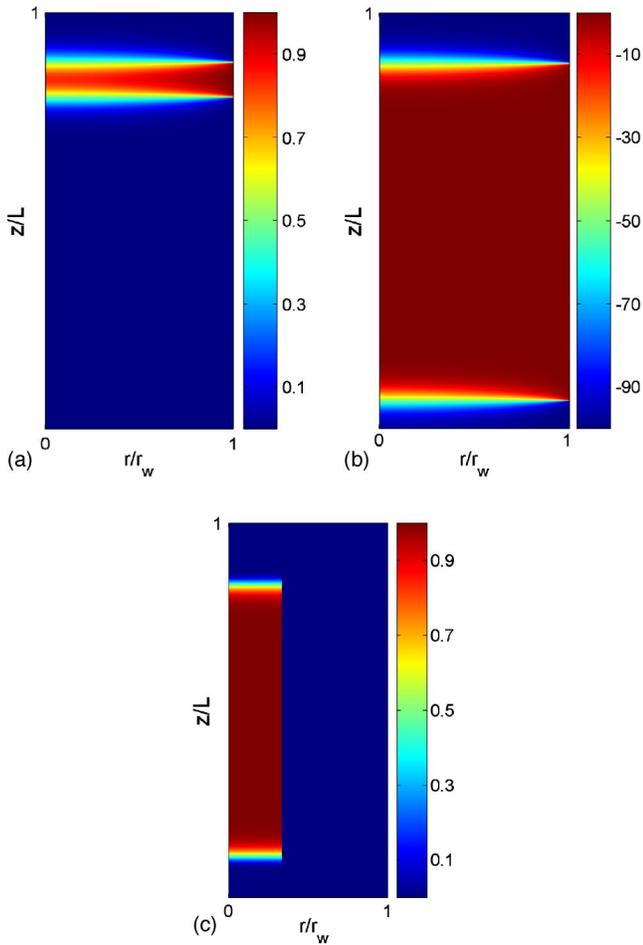
FIG. 1. (Color online). Plot of the (r,z) behavior of (a) the drive potential for a reference biasing voltage of 1 V, (b) the potential confining the plasma (both in volts), and (c) the initial equilibrium plasma density, normalized to its maximum value. (a) shows that the drive potential is very localized in z: it actually drops to zero at points a few r_w away from the biased drive electrode. For this reason, the interaction between the drive and the plasma is very limited in space.

$$\nabla^2\phi = \frac{e}{\varepsilon_0}\int f(r,z,v_z,t)dv_z,\tag{3}$$

where f_0 of Eq. (1) is the initial value for f in the Vlasov equation, and where ϕ_{dr}, ϕ_w are the drive potential and the well potential, respectively. The potentials ϕ_{dr}, ϕ_w satisfy the Laplace equation

$$\nabla^2\phi_{dr,w} = 0\tag{4}$$

with different boundary conditions, the two potentials being related to different biased gates. Figure 1 shows the (r,z) behavior of the potential well induced by the end electrodes and of the drive potential (due to the linearity of the Laplace equation, of course the solution for the drive has just to be rescaled for different drive amplitudes). In Eqs. (2) and (3) the radial coordinate enters only in the Poisson equation. This suggests that one can perform numerical studies of the evolution of the system by employing coupled one-dimensional codes, thus decreasing the computational effort with respect to a full 2D code.

For present purposes, the plasma can be generically regarded as a set of N_R "1D plasmas," located in different radial zones of the trap. Clearly, the radial extension of each of these zones has to be small enough so that a 1D, r-averaged description of the plasma is sufficiently close to the correct two-dimensional analysis. The evolution of these 1D systems are coupled via the Poisson equation for the self-consistent potential, and hence can be studied with N_R 1D-PIC codes.

More precisely, we considered a radial decomposition of the distribution function f:

$$f(r,z,v_z,t) \simeq \sum_{k=1}^{N_R} f_k^R(z,v_z,t)S_k(r),\tag{5}$$

where $\{S_k\}$ are b_0-spline functions, defining the distinct radial zones of the two-dimensional plasma distribution. Each of the N_R PIC codes allows the study of the evolution in time of the $\{f^R\}$ quantities. The presence of a grounded cylindrical electrode surrounding the plasma makes a Bessel expansion for the self-consistent potential particularly convenient for the solution of the Poisson equation:

$$\phi(r,z,t) = \sum_{k=1}^{N_B} \phi_k(z,t)J_0\left(\frac{j_{0k}}{r_w}r\right),\tag{6}$$

where j_{0k} is the kth zero of the J_0 Bessel function. A similar expansion has to be performed for the distribution function f by using an area-weighted average in r; the relation between the set of N_B Bessel coefficients $\{f^B\}$ and the $\{f^R\}$ coefficients in Eq. (5) is linear,

$$f_h^B = \sum_{k=1}^{N_R} \mathbf{M}_{h,k}f_k^R\tag{7}$$

and the coefficients are evaluated only once at the beginning of the simulation:

$$\mathbf{M}_{h,k} = \frac{2}{r_w^2 J_1^2(j_{0h})}\int_{r_k}^{r_{k+1}} J_0\left(\frac{j_{0h}}{r_w}r\right)rdr,\tag{8}$$

where r_k, r_{k+1} are the radii defining the kth radial zone. By doing so, a set of one-dimensional equation of the form

$$\frac{\partial^2\phi_k}{\partial z^2} - \left(\frac{j_{0k}}{r_w}\right)^2\phi_k = \frac{e}{\varepsilon_0}\int f_k^B(z,v_z,t)dv_z\tag{9}$$

has to be solved at each time step. Once the self-consistent potential has been obtained, the z component of the electric field is evaluated and averaged in r over the different radial zones, thus obtaining a set of one-dimensional self-fields $\langle E_z \rangle$; as said before, here the average is area weighted, but other possibilities can be considered. The same averaging is considered for the electric field of the confining well $E_{w,z}$ and for the drive field $E_{dr,z}$ at the beginning of the evolution. In this way, the study of the system has been completely reduced to coupled one-dimensional systems. For a generic, smoothly varying plasma radial profile, a few radial zones are expected to provide a very good description of the system: in fact, by properly arranging the radii delimiting the different radial zones, it is possible, in general, to reproduce
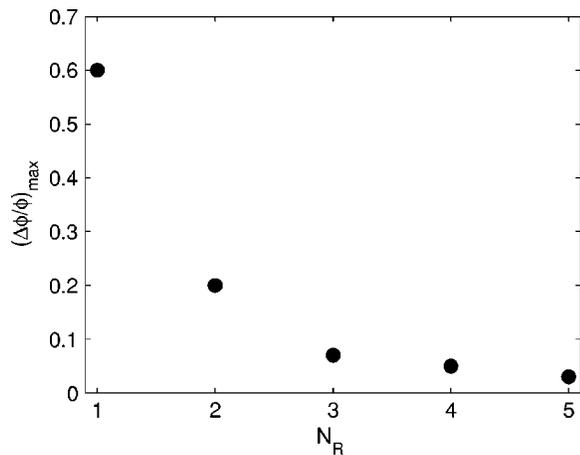
FIG. 2. Plot of the maximum relative error in the evaluation of the self-potential induced by the radial decomposition of the real plasma distribution [see Eq. (5)]. In this case, a Gaussian radial profile was considered, with a variance $\sigma = r_w/4$. The figure shows that the decomposition leads to large errors if one radial zone is considered. The situation drastically improves if few radial zones are added, and the error is ~3% for $N_R = 5$.

the potential generated by the correct plasma profile within a few percents of relative error. The self-potential is what deeply influences the evolution of the BGK structures under consideration, so a good estimate of the potential is desired in the simulations. For a Gaussian radial profile of variance $\sigma = r_w/4$, the dependence of the maximum relative error on the number N_R of considered radial zones is reported in Fig. 2. The figure shows that, for a generic radial profile, a radial average on the entire transverse section gives a poor estimate of the potential generated by the plasma. Nonetheless, a large improvement is achieved by considering two radial zones, and a maximum error of ~3% is obtained if $N_R = 5$. This means that, in general, the employment of a few radial zones gives a close estimate of the real plasma distribution. For this reason, a number of computational particles which is of the order of those employed in 1D simulations can be employed in this case as well, thus making the simulations particularly efficient.

III. SIMULATION PARAMETERS

In this section, some features of the code are discussed, along with some details concerning the numerical parameters adopted in the simulations.

A uniform grid in z has been chosen, with a spacing $\Delta z \lesssim \lambda_D$: this grid is fine enough to resolve properly the self-field acting on the plasma, but not for a good evaluation of the external fields $E_{w,z}$ and $E_{dr,z}$, which have strong spatial variation in z (see Fig. 1). In fact, tests performed by considering a single-particle motion in the potential well, with a *cloud-in-cell* (CIC) interpolation of the electric field on the particle,[11] have shown that a much finer grid has to be employed in order to preserve the energy of the particle for a high number of bounces, as desirable in the simulations. For this reason, we decided to use two distinct grids in the code. A "coarse" grid, with $\Delta z \lesssim \lambda_D$, is used as reference grid and in the evaluation of the plasma self-field, while a finer grid is used for the external potentials. By doing so, the total exter-

nal field $(E_{w,z} + E_{dr,z})$ acting on a single computational particle is obtained by a CIC interpolation of these fields on the finer grid. In this way, the energy of a particle bouncing back and forth is well preserved for a large number of oscillations.

Given the nature of the experiments, an accurate description of the motion of the particles initially resonant with the drive is very important, as well as the motion of all the particles that will interact strongly with the drive in the frequency-sweep process. For this reason, the time step Δt can be determined conservatively by imposing that the distance traveled in Δt by a particle initially resonant with the drive, $v_{res,0} \Delta t$, $(v_{res,0} \simeq \omega_d(t=0)L/\pi)$, be smaller than the grid size Δz.

However, in the system two well-separated time scales are involved, with important consequences on the computational effort required by the simulations. A fast time scale is associated with the fast oscillations of the drive or, equivalently, with the bounce motion of the electrons in the trap: in fact, in the experiments, the drive frequency $\omega_d(t)$ and the thermal bounce frequency of the electrons, $\Omega_{th} \equiv v_{th}\pi/L$, are such that $\omega_d \gtrsim \Omega_{th}$. The slow time scale of the system is related to the adiabatic chirp of the drive frequency. Typically, one has $\dot{\omega}_d/\omega_d^2 \sim 10^{-2}-10^{-3}$, the excitation process occurring at least over hundreds of oscillations.

For the simulations presented here, the following choice of parameters was adopted. $\Delta z = L/120$, $\Delta t = \Delta z(4v_{res,0})^{-1}$, $\Delta z_f = \Delta z/4$, $N_R = 1$ or 2, and $N_B = 7$ [see Eqs. (5) and (6)]. Simulations with higher N_R were performed with no appreciable variation in the results, as in our case r_p is considerably smaller than r_w and given the considered radial profile. Nonetheless, for plasma columns of larger radial extensions, higher values for these two parameters are necessary (an extended analysis of the sensitivity of the results to N_R, N_B for larger plasma columns is the object of a different paper).

IV. RESPONSE OF THE SYSTEM TO THE FREQUENCY-SWEEP DRIVE

The results of the simulations have been validated by direct comparison with experimental data. Here we report the results of a first set of simulations that were performed to calculate the response of the plasma to different drive amplitudes for different sweep rates of the drive. In all the simulations, the drive frequency is swept from $\omega_1 = 3$ MHz to $\omega_2 = 2.2$ MHz (as in Ref. 8): the velocity initially resonant with the drive is ~$2v_{th}$, while the resonant velocity at the end of the process is ~$1.5v_{th}$.

The computational time required per simulation is strongly dependent on the drive parameters considered in the excitation process: in general, the computational cost of a simulation increases for lower drive amplitudes. In fact, in this case the response of the plasma becomes significant for lower sweep rates, which are of course inversely proportional to the duration of the experiment for fixed $\omega_{1,2}$. In addition, more computational particles are required to resolve properly the effect of the drive on the plasma (in the simulations, up to ~10^5 computational particles where used).

The experiments[8] showed the existence of a rather sharp threshold in the sweep rate for a given drive amplitude, as
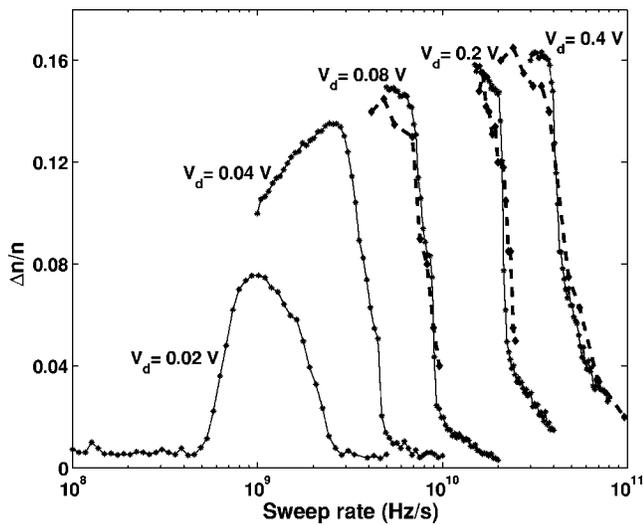
FIG. 3. Plot of the maximum response of the system as a function of the sweep rate for different drive amplitudes V_d. In all the different cases considered, the sweep range is $3-2.2$ MHz. The dashed lines have been obtained in the simulations while the solid lines are from experiments.

shown in Fig. 3. According to the analytical theory in Ref. 9, the maximum sweep rate, beyond which the response is expected to be very low, depends linearly on the drive amplitude. We analyzed the evolution in time of the radially averaged density at the end of the plasma column opposite to the drive gate, in the axial region of the trap considered in the experiments. In Fig. 3, a comparison with the results obtained in the experiments is presented, with a plot of the response of the system at the end of the excitation process for different drive amplitudes and sweep rates. As a precise knowledge of all the experimental conditions was not available, the results of a first simulation were scaled in order to match the experimental results. Then, the same scaling was considered for all the simulations that followed, and a remarkable agreement was found for a large range of variation of the drive parameters. For this reason, the results presented here are in a close quantitative agreement with the experiments, as opposite to the results of the simulations presented in Ref. 9, in which the values of some key simulation parameters (e.g., the drive amplitude and the length of the plasma column) were simply estimated, and which provided just preliminary results. From Fig. 3, one can see that the simulations confirmed the experimentally seen linear dependence of the threshold on the drive amplitude. Finally, as in experiments, the phase-space hole created in the plasma (see Fig. 4) is very robust and, in the simulations, lasts for several hundreds of bounce periods once the drive is switched off: this can be seen in Fig. 5(a), where the evolution in time of the density fluctuations is reported (in all the figures, time is normalized to the inverse of the thermal bounce frequency $\Omega_{th}=v_{th}\pi/L$). Figure 5(a) shows both the driven part of the evolution (in which the density fluctuations slowly grow in amplitude) and the undriven part (where the growth is arrested). The density variations associated with the electron hole constitute the BGK mode, as can also be seen in Fig. 5(b).
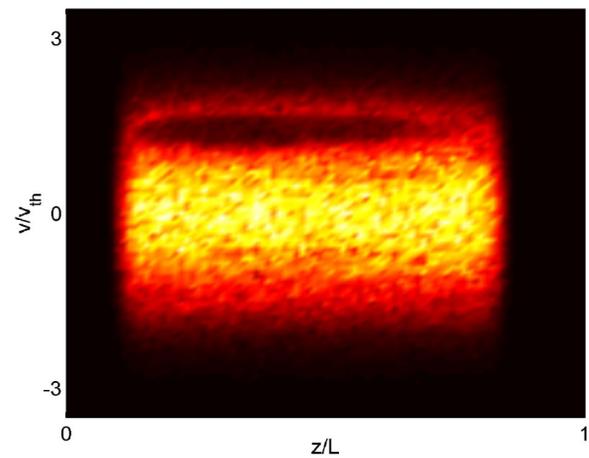

FIG. 4. (Color online). Phase-space plot of the normalized distribution function at the end of the driving process for a drive amplitude V_d of 0.2 V and a frequency range of $3-2.2$ MHz, with a sweep rate of 2.4×10^{10} Hz/s, showing the presence of the phase-space hole created by the drive.

V. PLASMA RESPONSE TO THE DRIVE AND GROWTH OF THE BUCKET

The code was also used to analyze in detail the response of the plasma to the drive and to study the process of formation and growth of the hole in the distribution function. We report the results of the excitation of the plasma with a drive amplitude of 0.4 V, with frequency swept from 3.5 MHz to 2 MHz with a sweep rate of 5×10^{10} Hz/s. This corresponds to an initial resonant velocity of $\sim 2.3 v_{th}$ and to a final resonant velocity of $\sim 1.3 v_{th}$.

In general, the drive potential has a high spatial harmonic content: for this reason, as discussed in Ref. 9, higher resonances can be expected, which are responsible for the
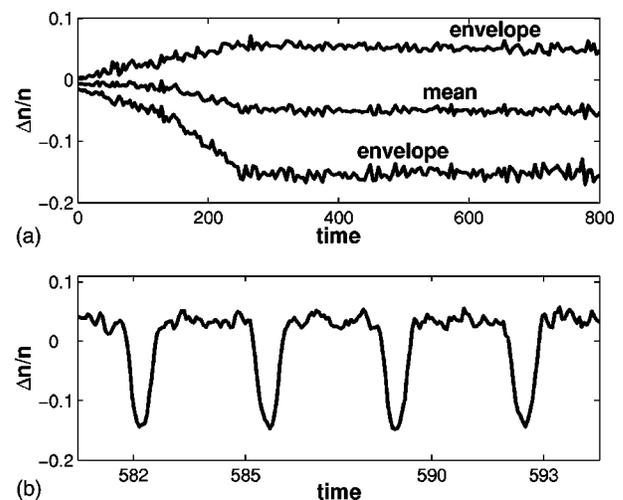

FIG. 5. (a) Plot of the evolution in time (normalized to $1/\Omega_{th}$) of the envelope and of the mean value of the normalized density fluctuations, as calculated in the simulations at one end of the plasma column. The plot comprises both the driven part of the evolution (in which the size of the bucket increases, as it is dragged down to lower velocities in phase space) and the undriven part, showing the persistence in time of the structure created by the drive. (b) Detail of the density oscillations, showing the typical pattern found in the experiments: each negative peak corresponds to a period of oscillation of the bucket along the plasma column.
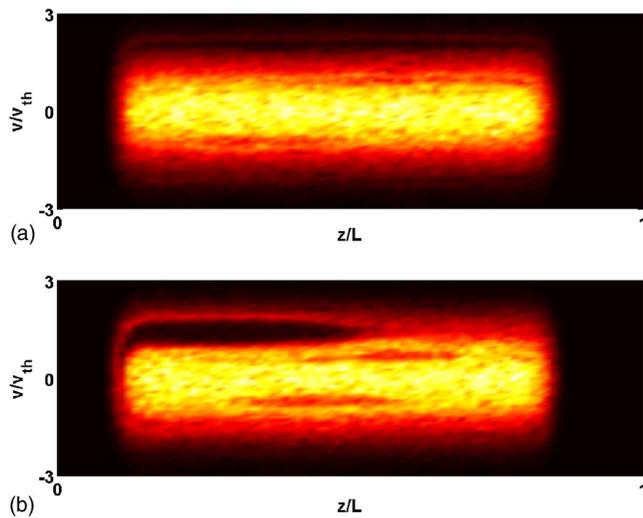
FIG. 6. (Color online). (a) Plot of the phase-space normalized distribution at the beginning of the evolution, $t \sim 70$ (i.e., after nearly 9 μs) and (b) almost at the end of the excitation process, $t \sim 200$ (after nearly 26 μs). In the first part of the evolution, the large bucket is visible in the upper part of the phase space: its length is almost equal to L_p, the length of the plasma column. At later times in the evolution, the small buckets, as well as the variation in shape of the large hole, are visible. Here, the drive amplitude V_d is 0.4 V and the frequency range considered is 3.5–2 MHz, with a sweep rate of 5 $\times 10^{10}$ Hz/s.
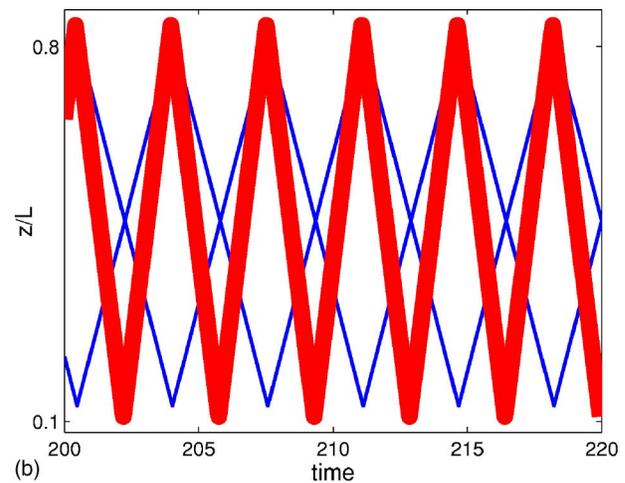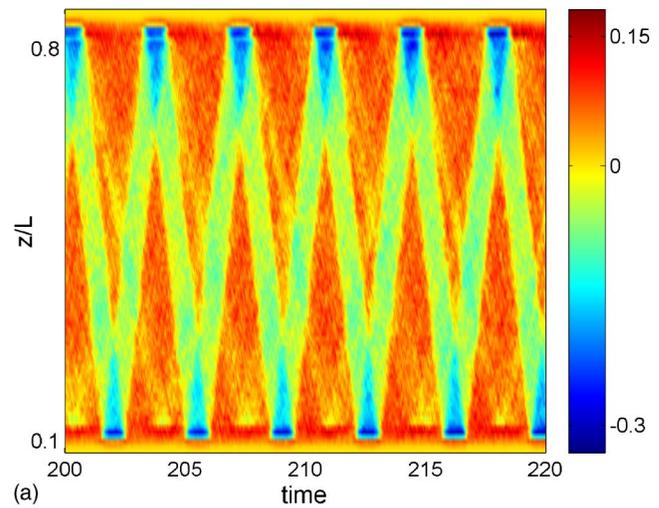

FIG. 7. (Color online). Detail of the time evolution of the deviation of the radially-averaged density field from its initial value, at the end of the driving process. In (a), the large band is a clear signature for the presence of the main hole bouncing back and forth in the trap. The density variations get larger at the turning points, where the bucket is more compressed in space, as evidenced by the darker zones in the upper and lower parts of the figure. Two narrower lines are also visible, indicating the presence of two smaller holes. The small buckets are particularly evident in the lower part of the figure because, while inverting their motion, they lead to larger density fluctuations, as shown by the brighter spots. Hence, the dynamics of the three holes leads to the pattern that is shown in (b), where the thicker line refers to the larger structure and the two narrower lines to the smaller ones.

formation of phase-space holes at lower velocities. Nonetheless, the amplitude of the higher drive harmonics is smaller than the fundamental one, and a shift of the resonant velocity $\Delta\omega/k_1$ for the fundamental resonance corresponds to a smaller shift for higher harmonics, $\Delta\omega/k_n$, being $k_n = nk_1$. For this reason, the excitation of these holes implies larger frequency sweep ranges and drive amplitudes. Higher resonances lead to the formation of smaller holes, at nearly half the velocity of the fundamental, which are barely visible in Fig. 4, but which become clearly visible if a higher drive amplitude is considered (Fig. 6). In the first part of the driving process, only the large hole is clearly visible: its initial length is roughly equal to the length of the plasma column [Fig. 6(a)]. At later times, the smaller holes become more prominent and the larger hole, while growing and slowly drifting into the bulk of the distribution, slowly changes its shape. In fact, as its length slowly decreases, it gets wider in velocity [see Fig. 6(b)], thus causing higher density perturbations.

The growth of the density fluctuations is arrested when the drive is switched off (this occurs at the normalized time $t \sim 228$): nonetheless, the structure created in the plasma by the drive persists in time for many bounce periods, as also previously shown in Fig. 5. From Fig. 6, one can see that, in both the driven and in the undriven part of the evolution, the two small holes bounce back and forth with different frequency with respect to the large hole. This can be seen also by examining the time evolution of the deviation of the density field from its initial value, as reported in Fig. 7.

In Fig. 7(a), the quantity $[n(z,t) - n_0(z)]/\langle n_0 \rangle$ is reported, $\langle n_0 \rangle$ being the mean value of the initial density distribution: the driven evolution occurs in roughly a hundred bounce periods, and just a detail of the last part of the driven evolu-

tion is reported. The large band, clearly visible, is determined by the presence of the large BGK hole bouncing back and forth in the trap. In the figure, besides the large BGK structure, the presence of two smaller structures is evident: two, narrower lines create two periodic patterns with a period twice as large as the period of the fundamental structure. These lines become particularly evident when the small structures, inverting their motion, lead to density perturbations of larger entity. This occurs at the turning points and is represented, in the lower part of the figure, by clearly visible bright spots: in fact, in this case, the inversion of motion occurs when the larger structure is in a different part of the trap. In the upper part of the figure, the inversion of the smaller structures occurs simultaneously with the inversion of the larger one, and the density fluctuations are dominated
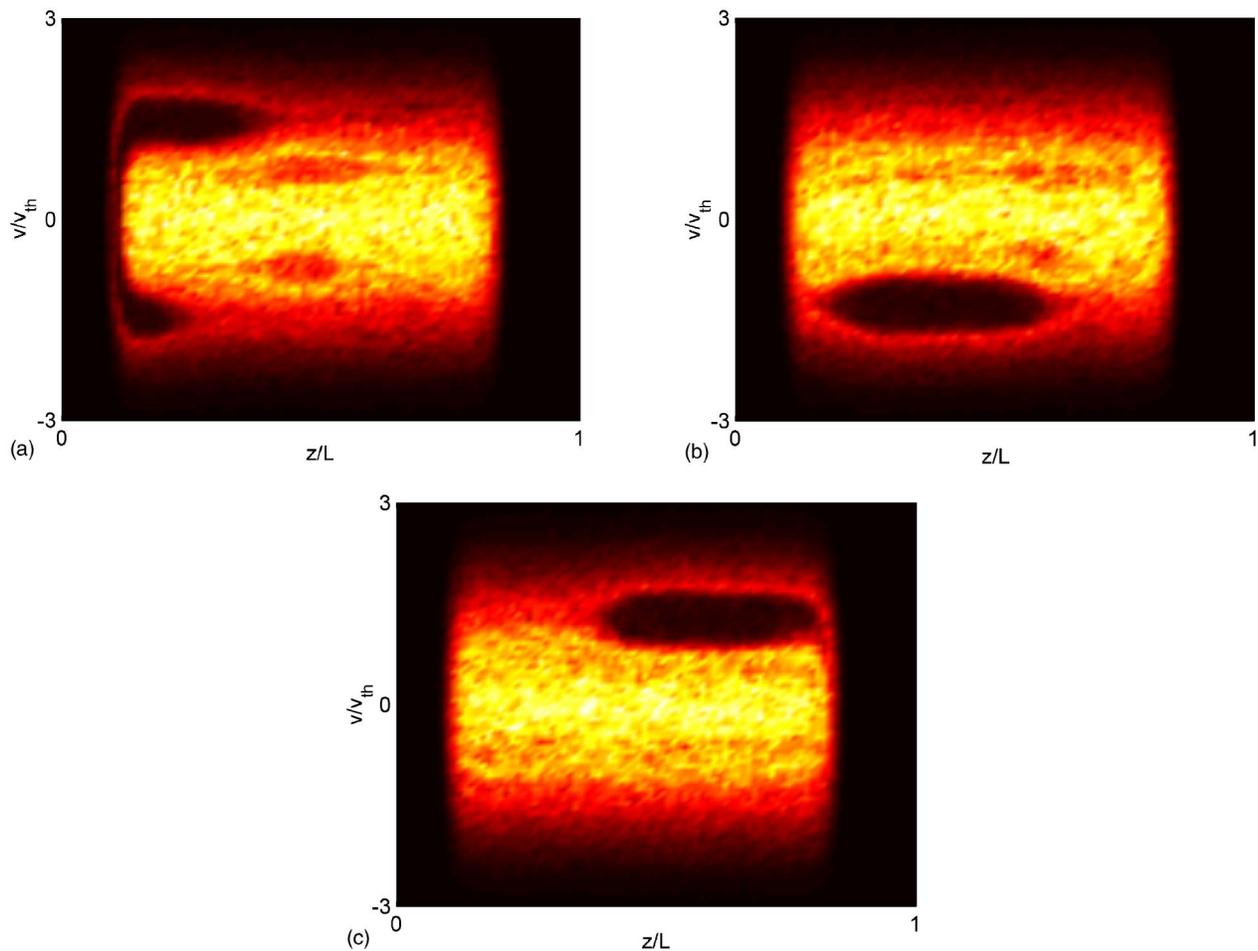
FIG. 8. (Color online). Plot of the phase-space normalized distribution during (a) the final part of the driven evolution and during the undriven evolution, after nearly (b) 12 and (c) 30 periods of oscillation of the large hole.

by the larger structure. The dynamics discussed here defines, in Fig. 7(a), the pattern which is reported in Fig. 7(b).

During the driven evolution, the gap in velocities between the large and the small holes gets narrower: the holes get wider in velocity, and the large hole drifts toward lower velocities twice as fast as the smaller ones. For this reason, two distinct holes (a large and a small one) can get very close in phase space. When this occurs, the large hole can deform the small one, but the interaction is limited and the small structure is preserved as long as the drive is on [Fig. 8(a)]. This is no longer true in the undriven part of the evolution. After ≈ 15 undriven bounce periods of the large hole, the small structures have almost disappeared, and after nearly 25 periods they have been completely absorbed by the larger structure: the distribution reaches a stable configuration which is slightly different from the one present at the moment the drive was turned off, and in which just one large coherent structure is present [Figs. 8(b) and 8(c)].

This can also be seen in Fig. 9: here, the same evolution as reported in Fig. 7 is reported for the undriven evolution, after 25 undriven periods of the large hole. The figure shows that the two, narrower lines, associated with smaller structures in Fig. 7(a), have disappeared. Though, during the undriven evolution of the plasma, the small structures are not always destroyed in a few bounce periods of the main

hole: if the gap in velocity between the large and the smaller holes is wider, they can survive for a higher number of bounces. This situation is shown in Fig. 10(a): in this case, the plasma was driven with the same drive amplitude and chirp rate, but within a smaller drive frequency range (from
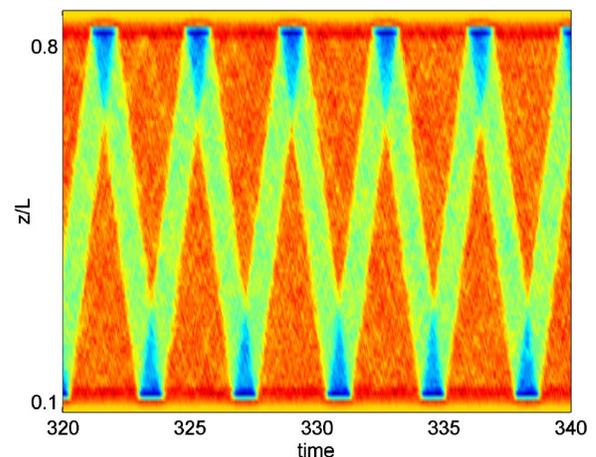

FIG. 9. (Color online). Same as Fig. 7(a), but after 25 bounce period of the undriven large hole, showing that the smaller structures have been destroyed by the interaction with the larger structure.
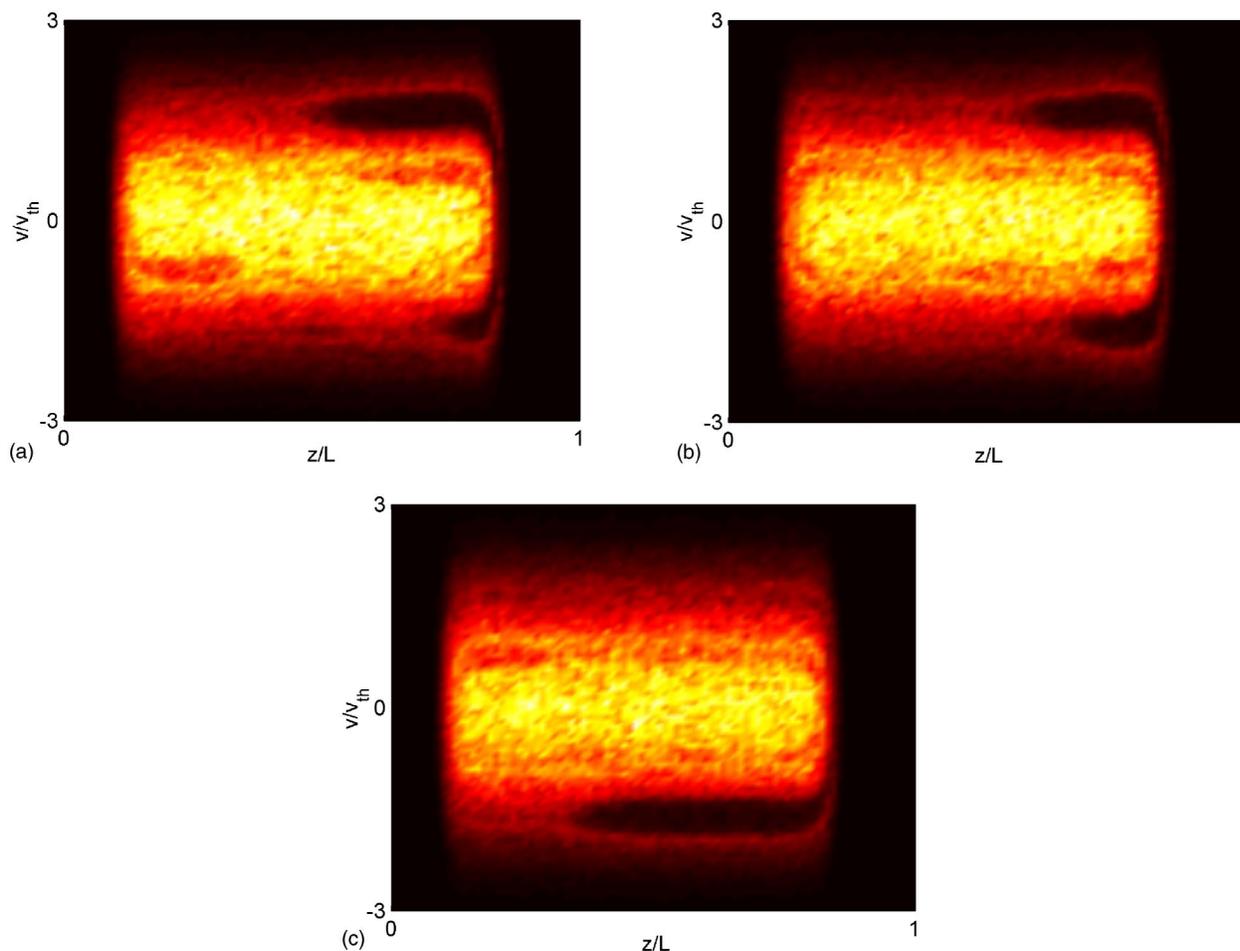
FIG. 10. (Color online). Response of the system for a drive amplitude of 0.4 V, sweep rate of 5×10^{10} Hz/s, from 3.5 MHz to 2.5 MHz. (a) Phase-space portrait of the system at the end of the driving process and after (b) 60 and (c) 95 undriven periods of oscillation of the large hole.

3.5 MHz to 2.5 MHz). Figure 10(a) shows the phase-space portrait of the system at the end of the driving process, while Figs. 10(b) and 10(c) show the same quantity after 60 and 95 periods of oscillation of the main hole, respectively. In this case, at the end of the driven evolution, the large and the small structures are well separated in velocity. The interaction between the small and the large holes is weaker than the one observed in the previous case (see Fig. 8), and the two small structures are still present in the distribution after nearly a hundred bounce periods of the large hole.

VI. CONCLUSIONS

We have discussed an efficient way to perform numerical studies on the longitudinal dynamics of axisymmetric pure-electron plasmas confined in a Penning trap: starting from the full 2D model of the system, the presence of a strong axial magnetic field allows for a decomposition of the original system into a set of coupled 1D systems. In this way, the important 2D features of the real system are taken into account precisely in the numerical model. We used this ap-

proach to study the excitation of synchronized BGK modes in these plasmas by chirped frequency drives: as already shown in previous experiments, a weak oscillating drive with slowly chirped frequency can induce large phase-space holes in the plasma. These coherent structures are responsible for density fluctuations of large amplitude, and can last for thousands of bounce periods in the trap in the absence of the drive. We compared the results of simulations with the experimental observations, finding an excellent agreement. We also observed the interaction of the large, main hole with smaller structures due to higher-order resonances between the plasma and the drive. While the drive is on, this interaction is limited and the small structures are preserved. In the subsequent undriven evolution, the smaller structures strongly interact with the main one, and the plasma slowly evolves towards an equilibrium configuration in which just one large structure is present. Further investigations should examine the interaction between distinct structures in the undriven part of the evolution, especially in the case of structures of the same size. Also, more complex BGK-type structures involving phase-space holes localized in both axial coordinate z and azimuthal angle θ can be envisioned in these plasmas. However, because of the large disparity of the

time scales characterizing the axial and azimuthal dynamics (the latter being governed by slow $\mathbf{E} \times \mathbf{B}$ drifts of plasma electrons), it would be difficult to include azimuthal dynamics in the present numerical model. In the experiments discussed here and in Refs. 8 and 9, such three-dimensional structures were not observed, because of the high level of axisymmetry in the drive. Nevertheless, the possibility of resonant excitation of nonaxisymmetric BGK modes in trapped pure-electron plasmas seems to be an interesting goal for future work.

ACKNOWLEDGMENTS

[1] I. B. Bernstein, J. M. Greene, and M. D. Kruskal, Phys. Rev. **108**, 546 (1957).
[2] H. Schamel, Phys. Plasmas **7**, 4831 (2000).
[3] C. B. Warton, J. Malmberg, and T. O'Neil, Phys. Fluids **11**, 1761 (1968).
[4] J. D. Moody and C. F. Driscoll, Phys. Plasmas **2**, 4482 (1995).
[5] G. Hart and B. G. Peterson, in *Non-Neutral Plasma Physics IV: Workshop on Non-Neutral Plasma*, edited by F. Anderegg, C. F. Driscoll, and L. Schweikhard (AIP, New York, 2002), p. 341.
[6] W. L. Kruer, J. M. Dawson, and R. N. Sudan, Phys. Rev. Lett. **23**, 838 (1969).
[7] J. Danielson, Ph.D. thesis, University of California, San Diego, 2002.
[8] W. Bertsche, J. Fajans, and L. Friedland, Phys. Rev. Lett. **91**, 265003 (2003).
[9] L. Friedland, F. Peinetti, W. Bertsche, J. Fajans, and J. Wurtele, Phys. Plasmas **11**, 4305 (2004).
[10] A. Trivelpiece and R. Gould, J. Appl. Phys. **30**, 1784 (1959).
[11] C. K. Birdsall and A. B. Langdon, *Plasma Physics via Computer Simulation* (McGraw-Hill, New York, 1985), p. 65.